RESEARCH ARTICLE

NANO · MICRO small
www.small-journal.com

Large Enhancement of Polarization in a Layered Hybrid Perovskite Ferroelectric Semiconductor via Molecular Engineering

Na Wang, Ning Ding, Ze-Jiang Xu, Wang Luo, Hua-Kai Li, Chao Shi, Heng-Yun Ye, Shuai Dong, and Le-Ping Miao**

Switchable spontaneous polarization is the vital property of ferroelectrics, which leads to other key physical properties such as piezoelectricity, pyroelectricity, and nonlinear optical effects, etc. Recently, organic–inorganic hybrid perovskites with 2D layered structure have become an emerging branch of ferroelectric materials. However, most of the 2D hybrid ferroelectrics own relatively low polarizations (<15 μC cm^{-2}). Here, a strategy to enhance the polarization of these hybrid perovskites by using *ortho*-, *meta*-, *para*-halogen substitution is developed. Based on (benzylammonium)$_2$PbCl$_4$ (BZACL), the *para*-chlorine substituted (4-chlorobenzylammonium)$_2$PbCl$_4$ (4-CBZACL) ferroelectric semiconductor shows a large spontaneous polarization (23.3 μC cm^{-2}), which is 79% larger than the polarization of BZACL. This large enhancement of polarization is successfully explained via ab initio calculations. The study provides a convenient and efficient strategy to promote the ferroelectric property in the hybrid perovskite family.

1. Introduction

Ferroelectric materials have received great attention due to the extensive applications in various technologies, such as sensors, switches, nonvolatile storage and photoelectric devices etc.[1–5] 3D inorganic ferroelectrics have been commercially popular, such as $BaTiO_3$.[6–8] In the meantime, organic–inorganic hybrid perovskites (HOIPs) have emerged as a new class of ferroelectric materials with the features of easy synthesis, lightweight, structural diversity, and low cost.[9–11] Moreover, the ferroelectric properties of some hybrid ferroelectrics are comparable to inorganic ferroelectrics.[12] Among these hybrid ferroelectrics, 2D hybrid perovskite ferroelectrics are an important member. As well known, they have no restriction of the Goldschmidt's tolerance factor compared to the 3D hybrids. Because their enormous structural tunability makes the inorganic 2D layers to allow maximum inclusion of diverse organic components, such as aliphatic amines or aromatic amines, etc. These organic components adopt a polar directional arrangement resulting in ferroelectric orders. Besides, based on the superior environmental stability, 2D hybrid perovskite's ferroelectric polarization is benefitting for the development of many optoelectronic devices with unprecedented characteristics.[13–17] Of which, 2D Sn (II), Ag (I)-Bi (III) or Pb (II) based hybrids commonly exhibit remarkable electronic or optical properties owing to the quantum-well electronic structure, representing a class of technically important semiconductor materials. More importantly, combining the ferroelectricity and semiconductor properties means previously unknown photophysical phenomena or light control ferroelectric behavior, such as polarization coupled X-ray detection, self-driven photodetection, etc.[18–22] As well known, switchable spontaneous polarization (P_s) is the origin of ferroelectricity. Especially, the value of P_s is the critical factor for the ferroelectric performance.[21,23,24] However, the reported cases of 2D layered hybrid ferroelectrics with large P_s is much smaller compared to the inorganic ferroelectric ($BaTiO_3$, 26 μC cm^{-2}),[6] such as [4,4-difluoropiperidinium]$_4$AgBiI$_8$ (10.5 μC cm^{-2}),[19] [Benzylamium]$_2$[PbCl$_4$] ((BZA)$_2$PbCl$_4$/BZACL, reported maximum, 13 μC cm^{-2}),[25] and [(C$_4$H$_9$NH$_3$)$_2$(NH$_3$CH$_3$)]$_2$[Sn$_3$Br$_{10}$] (11.8 μC cm^{-2}),[26] etc. Therefore, it has great scientific significance to promote the P_s of ferroelectric semiconductor materials.

According to the structural features of 2D hybrid perovskites, organic components can easily regulate the internal structures of the 2D HOIPs because the size or conformation of the organic cations with strong influence on the distance or dislocation of metal-halide layers, and connection mode of the metal-halide octahedron.[13,17,27] Therefore, the rational design or compositional engineering on the organic parts will provide a promising avenue to achieve high-performance of 2D hybrid ferroelectrics,

N. Wang, Z.-J. Xu, W. Luo, H.-K. Li, C. Shi, H.-Y. Ye, L.-P. Miao
Chaotic Matter Science Research Center, Department of Materials Metallurgy and Chemistry
Jiangxi University of Science and Technology
Ganzhou 341000, China
E-mail: miaoleping@jxust.edu.cn

N. Ding, S. Dong
Key Laboratory of Quantum Materials and Devices of Ministry of Education
School of Physics
Southeast University
Nanjing 211189, China
E-mail: sdong@seu.edu.cn

The ORCID identification number(s) for the author(s) of this article can be found under https://doi.org/10.1002/smll.202306502

DOI: 10.1002/smll.202306502

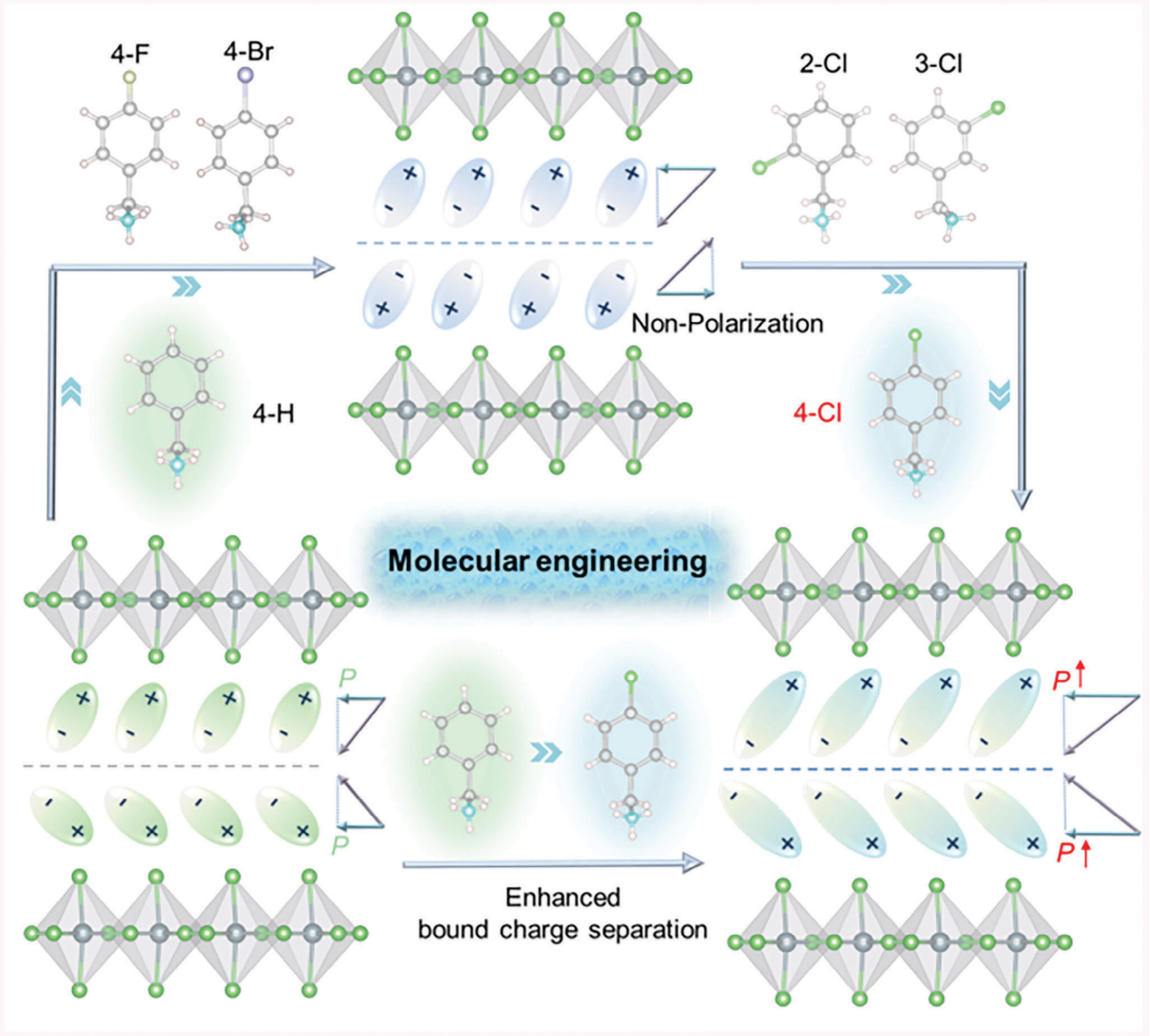

Scheme 1. Molecular engineering regulates the bound charge separation of organic cations to promote the Ps based on 2D hybrid perovskite ferroelectrics.

such as large P_s. At present, halogen substitution on the organic parts is one of the most powerful strategies to regulate the nature of the hybrid perovskites.[28,29] Herein, we designed a molecular engineering strategy for halogen substitution at different sites of organic cation to achieve the goal of promoting P_s. Based on the reported 2D hybrid ferroelectric BZACL, we investigated the effects of *ortho*-, *meta*-, and *para*-halogen substitution at benzylamium cation on P_s. As expected, the P_s of *para*-chlorine substituted (4-chlorobenzylammonium)$_2$PbCl$_4$ ((4-CBZA)$_2$PbCl$_4$/4-CBZACL) increases to 23.3 μC cm^{-2} showing great promotion comparing with the 13 μC cm^{-2} of BZACL (**Scheme 1**). This large P_s is the recorded maximum value in the 2D HOIPs system. Besides, 4-CBZACL shows an X-ray detection response with clear switching characteristics that light current 8.1 and dark current 0.5 pA cm^{-2}. This study will provide an effective pathway for designing large P_s ferroelectrics and exploring ferroelectric semiconductor materials, such as photoferroelectrics.

2. Results and Discussion

2.1. Analysis of the Single-Crystal Structures

The plate-like crystals of these 2D lead based hybrid compounds were obtained from a saturated solution (see the supporting information). The phase purity of 4-CBZACL was verified by powder X-ray diffraction (PXRD) (Figure S1, Supporting Information). Thermogravimetric (TG) analysis shows the thermal

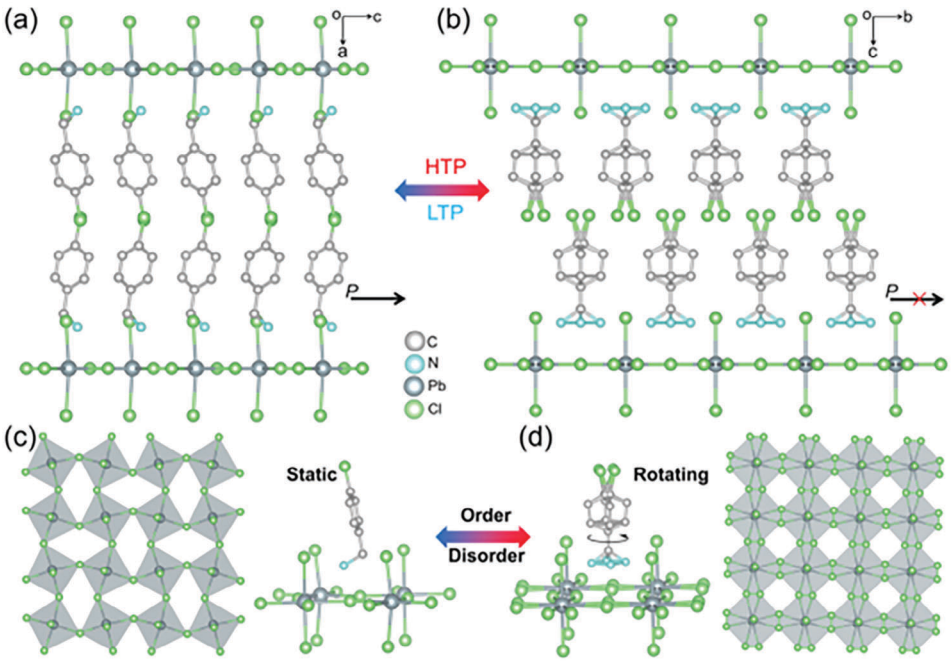

Figure 1. The single-crystal molecular structures of 4-CBZACL. a) The 2D layered packing structure in LTP along *c* axis. b) 2D layered packing structure in HTP along *b* axis. c) The top view of 2D inorganic framework and static state of organic cations in LTP. d) The rotating state of organic cations and top view of 2D inorganic framework and in LTP. For clearly, the H atoms were hidden.

stability of 4-CBZACL was up to 441 K. (Figure S2, Supporting Information). First, all of the single-crystals of the hybrids were collected around the room temperature. They all maintained the 2D layered structure similar to BZACL (Figures S3–S6, Supporting Information). While, FBZACL, BBZACL, 2-CBZACL, and 3-CBZACL all crystallize in centrosymmetric space groups *Pnma*, *Pccn*, *Pnma*, and $P2_1/n$, respectively (Tables S1 and S2, Supporting Information). Notably, 4-Cl substituted hybrid 4-CBZACL still adopts the polar space group. Then, the variable temperature single-crystal structures of 4-CBZACL were collected to understand the molecular mechanism of phase transition and halogen substitution regulating intermolecular interaction. In the low-temperature phase (LTP) at 303 K, 4-CBZACL crystallizes in orthorhombic polar space group $Cmc2_1$ with a = 36.3722 (19) Å, b = 7.8297(4) Å, c = 7.7310(4) Å (Table S3, Supporting Information). 4-CBZACL is a typical A_2BX_4 2D organic–inorganic hybrid perovskite structure. It consists of the organic parts halogen substituted 4-Chlorobenzylamium cations and inorganic components corner-sharing $PbCl_6$ octahedron. In which, organic cations located in the inorganic 2D layers through the hydrogen bonding between $-NH_3^+$ and halogen (**Figure 1**a). Notably, the polar array of 4-chlorobenzylammonium along the *c* axis induces the polarization of 4-CBZACL. When in HTP, 4-chlorobenzylammonium rotating around the central axis itself shows a quadruple orientation disordered state resulting in 4-CBZACL adopts the higher symmetry space group I4/mmm (Figure 1b; Table S3, Supporting Information). To satisfy the high symmetry site, the inorganic anionic framework also exhibits orientation disorder. The synergistic order-disorder motions of organic components and inorganic layers result in the disappearance of polarization of 4-CBZACL. These differences also are supported by the changes in the minimum asymmetric unit and the bond lengths and angles of the metal-halide framework (Figures S7, S8, and Tables S4, S5, Supporting Information). In addition, this internal cooperative molecular motion should be the molecular basis which triggers its structural phase transition. Besides, Hirshfeld surface analysis[30,31] shows stronger hydrogen bonding interactions between organic cations and inorganic parts compared to BZACL (Figure S9, Supporting Information). Therefore, the motional energy barrier between the cations and anions has an increase resulting in the enhancement of phase transition temperature (T_c). In order to compare the effects of different halogen-substituted cations on inorganic 2D skeleton, the 4-CBZACL, FBZACL, and BBZACL were selected as the examples. First, the connection modes of the corner-sharing octahedron show obvious differences (Figure S10a, Supporting Information). In which, the four angles of the octahedron of 4-CBZACL are all different at 125.7°, 60.61°, 56.12°, and 117.31° respectively unlike FBZACL and BBZACL. Also, the dislocation of the 2D layers displays evident disparity along the direction of top view (Figure S10b, Supporting Information). Moreover, to understand the deviation of the metal-halide octahedrons, we provided the octahedral distortion parameters in low-temperature phase.[32] Of which, 4-CBZACL shows larger octahedral distortion that σ_1^2 = 23.11, σ_2^2 = 125.88, and $\langle\lambda\rangle$ = 1 (Here, σ_1^2 terms as angular distortion, σ_2^2 as the B-cite off-center displacement parameter, and $\langle\lambda\rangle$ as bond length quadratic elongation). The octahedral symmetry of 4-CBZACL involves a tetragonal–orthorhombic phase transition, both σ_1^2 and σ_2^2 = 0 in high-temperature phase due to the angles of Pb—Cl 90° and Cl—Pb—Cl 180°.

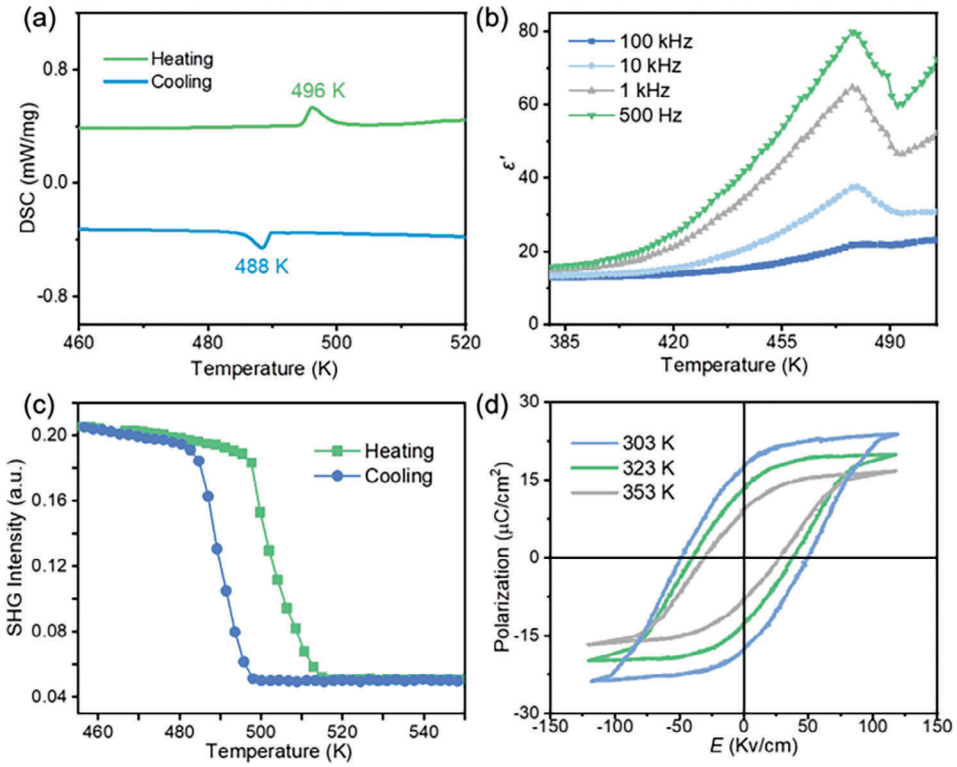

Figure 2. The ferroelectric phase transition of 4-CBZACL. a) DSC curves ≈460–530 K. b) dielectric anomaly at multiple frequencies (500 Hz, 1 kHz, 10 kHz, 100 kHz) upon variable-temperature. c) Evolution of SHG intensity in a heating and cooling run. d) Temperature dependence of *P–E* hysteresis loops at 50 Hz.

These indicate that the enhanced tendency of the stereochemical expression of the ns^2 electron pair will lead to B- cite ions off-centre displacement inducing breaking of inversion symmetry and then resulting in ferroelectricity in 2D lead-based halide perovskites.

2.2. Semiconductor Property

First, the bandgap 3.63 eV of 4-CBZACL was determined by UV–vis absorption spectroscopy (Figure S11 a, Supporting Information). Further, the bandgap characteristic of 4-CBZACL was performed by the theoretical calculations. As shown in Figure S11b (Supporting Information), the bottom of the conduction band (CBM) and the top of the valence band (VBM) are not both located at the G point, indicating the indirect bandgap. And the DFT calculated bandgap is ≈3.3 eV. The origin of the bandgap of 4-CBZACL was revealed by partial densities of states (PDOS) calculation. Moreover, we carried out the photoelectric response of 4-CBZACL upon X-ray irradiation based on the tableted sample (Figure S11c, Supporting Information). The detection performance of the device displays an X-ray response of dark/light current switch ratio 0.5 pA / 8.1 pA (Figure S11c, Supporting Information). This result shows the conductance under light achieves up to 16 times of under dark condition. More importantly, the good off-on switch also reveals the X-ray response property. Thus, all these indicate 4-CBZACL with a certain X-ray response for the potential application in semiconductor materials.

2.3. Proof of Ferroelectricity

Differential scanning calorimetry (DSC) measurement was performed to confirm the structural phase transition of 4-CBZACL. As shown in **Figure 2**a, and Figure S12 (Supporting Information), a pair of reversible endothermic and exothermic peaks around 496/488 K was clearly observed upon heating/cooling processes. The obvious thermal hysteresis of 8 K indicates a first-order phase transition of 4-CBZACL. Notably, this phase transition temperature (T_c) increased by 58 K compared to BZACL[25] is attributed to the halogen substitution enhancing the intermolecular motional energy barrier.

The structural phase transition is typically accompanied by a significant dielectric anomaly near T_c, which is generally consistent with the findings of DSC results.[33] Thus, we recorded the temperature-dependent traces of the real part (ϵ') of the complex dielectric constant on pressed powder pellets of 4-CBZACL. As demonstrated in Figure 2b, the ladder-shaped dielectric anomalies can be clearly observed upon the whole heating and cooling process, which proves that 4-CBZACL indeed undergoes a reversible structural phase transition. Second harmonic generation (SHG) measurement is a useful tool to prove the non-centrosymmetric structure of molecular crystals. Therefore, we collected the temperature-dependent SHG signals of 4-CBZACL in the range of 455–550 K as shown in Figure 2c. The results show that the SHG intensity displaying an obvious decrease ≈496 K in the cooling/heating process, which is consistent with the symmetry requirements of centrosymmetric paraelectric phase

Table 1. The Tc and the Ps of the reported cases based on 2D hybrid perovskites and this work.

Materials[a)]	T_c [K]	P_s [μC cm^{-2}]	References
$(4,4\text{-DFHHA})_2PbI_4$	454	1.1	[38]
$(PFBA)_2PbBr_4$	440	4.2	[39]
$[(R)\text{-}\beta\text{-MPA}]_2CdCl_4$	300	4.65	[37]
$(IA)_2(MA)_2Pb_3Cl_{10}$	343	≈5	[35]
$BA_2EA_2Pb_3Br_{10}$	380	≈5	[36]
$(ATHP)_2PbBr_4$	503	5.6	[41]
MHy_2PbBr_4	351	5.8	[43]
$(4AMP)PbI_4$	352	9.8	[40]
$(4,4\text{-DFPD})_2PbI_4$	428.5	10	[42]
$(4,4\text{-DFPD})_4AgSbI_8$	414	10.5	[19]
$(C_4H_9NH_3)_2(NH_3CH_3)_2Sn_3Br_{10}$	318	11.76	[26]
$(BZA)_2PbCl_4$	438	13	[25]
R-LIPF	483	13.96	[44]
$(4\text{-CBZA})_2PbCl_4$	496	23.3	This work

[a)] 4,4-DFHHA= 4,4-difluorohexahydroazepine; PFBA = perfluorobenzylammonium; MPA+ = methylphenethylammonium; (IA)2(MA)2 = [(CH3)2CH(CH2)2NH3]-2(CH3NH3)2; BA2EA2 = (C4H9NH3)2(C2H5NH3)2; ATHP = 4-aminotetrahydropyran; 4AMP = 4-(aminomethyl)piperidinium; MHy = Methylhydrazinium; 4,4-DFPD = 4,4-difluoropiperidinium; R-LIPF = [R-1-(4-chlorophenyl)ethylammonium]; BZA = benzylammonium; 4-CBZA = 4-Cl-benzylammonium.

(*I4/mmm*) and polar ferroelectric phases ($Cmc2_1$). The symmetry change $Cmc2_1 \rightarrow I4/mmm$ of 4-CBZACL from LTP to HTP belongs to 88 types of ferroelectrics with an Aizu notation of $4/mmmFmm2$.[34] Therefore, the polarization-electric field (*P*–*E*) hysteresis loops (variable-temperature) of the thin single crystal sample were performed to demonstrate the ferroelectricity of 4-CBZACL. As shown in Figure 2d, the typical *P*–*E* hysteresis loops of 4-CBZACL can be obtained at 303, 323, and 353 K. Remarkably, the obtained saturate polarization (P_s) at 303 K is estimated to be 23.3 μC cm^{-2}, which is the largest in reported hybrid 2D layered perovskite ferroelectrics (**Table 1**).[19,25,26,35–43] This reveals that spontaneous polarization value increases up to 179% after *para*-Cl substitution.

Besides, the ferroelectric domain structure and switching polarization of 4-CBZACL were further investigated by piezoresponse force microscopy (PFM) based on the thin single crystal, providing a deep insight of ferroelectricity on the nanoscale level. The amplitude and phase parameters of PFM images reflect the absolute magnitude of the local piezoelectric response and the polarization direction of the domains, respectively (**Figure 3**; Figure S13, Supporting Information). As shown in Figure S13 (Supporting Information), it can be observed that the domains are separated by a clear domain wall in vertical PFM. Besides, the domain structure of the lateral PFM is identical to that of vertical PFM. The existence of domains is a direct evidence of ferroelectricity for 4-CBZACL. To further verify the switchable ferroelectric polarization of 4-CBZACL, we conducted polarization switching tests by PFM measurements. As shown in Figure 3d,g, the distinct 180° reversal of phase signal and hysteresis amplitude-bias butterfly loops can be observed on the plane of a single crystal, which is a typical demonstration for the switching of ferroelectric polarization. To visualize the domain switching process, we performed local polarization tests. Figure 3i shows a single-domain region at the initial state. Subsequently, the positive bias of +100 V was applied over the region marked as a yellow dashed box. The newly generating domain is created by the polarization switching. Furthermore, the written green domain was reversed by applying an opposite voltage of −90 V over the area marked with a smaller yellow box. Ultimately, a box-in-box domain pattern was formed which further confirms the ferroelectric nature of 4-CBZACL.

2.4. Regulation Mechanism of Spontaneous Polarization

According to the single crystal structures and experimental evidence, the ferroelectric spontaneous polarization of 4-CBZACL is relevant to the polar array of the organic components. This also can be determined by the density functional theory (DFT) calculations. As shown in **Figure 4**, the P_s of this layered hybrid ferroelectric is 23.9 μC cm^{-2} according to the Berry Phase method of DFT calculation which matches with the experimental value. What's more, we also performed the DFT calculation with spin-orbit coupling (SOC), which still leads to a polarization of 23.9 μC cm^{-2}. The influence to ferroelectric polarization is negligible, in the order of 0.01 μC cm^{-2}. This phenomenon can be understood from the fact that the contribution of Pb atoms near the Fermi energy is very small (shown in Figure S14, Supporting Information), which implies that the SOC effect of Pb atoms has little influence to the physical properties of 4-CBZACL.

In order to estimate the different contributions of halogen-substituted organic cations and layered inorganic parts. The organic molecular is kept in the ferroelectric state and the inorganic ions are restored from the ferroelectric to the paraelectric state gradually, characterized by the normalized displacement as shown in Figure 4a, the polarization increases with the decrement of displacement distortion. The final polarization of 25.8 μC cm^{-2} is the pure contribution from halogen-substituted organic cations, and the contribution from the layered inorganic part can be derived as −1.8 μC cm^{-2}.

In addition, we also used another approximation to partition the individual contributions to net polarization. The organic cation is calculated separately. To mimic its positive charged state, holes are added during the calculation.[44] The polarization of organic cations is estimated to be 25.8 μC cm^{-2}, in consistent with the above result ideally.

Also, the DFT calculation of the P_s of BZACL was carried out. The calculated value of 13.4 μC cm^{-2} is very close to the actual result (Figure S14, Supporting Information). Thus, our theoretical calculation is reliable, which reveals 179% increasement of P_s via chloric substitution on the organic component.

Based on the DFT calculations, organic parts contribute the most of the polarization. We performed further investigation of chlorine atom substituted effect on P_s. In order to further reveal the influence of the rotation angle of the molecule on the dipole moment, the halogen-substituted organic cations are rotated in the *bc*-plane and the inorganic ions are distorted simultaneously, where the two molecules in the same layer are rotated in the opposite directions expect for $\theta = 90°$. As depicted in Figure 4b, the rotation of molecules changes the projection direction of dipole moments on the *bc*-plane. In addition, the polarization projection

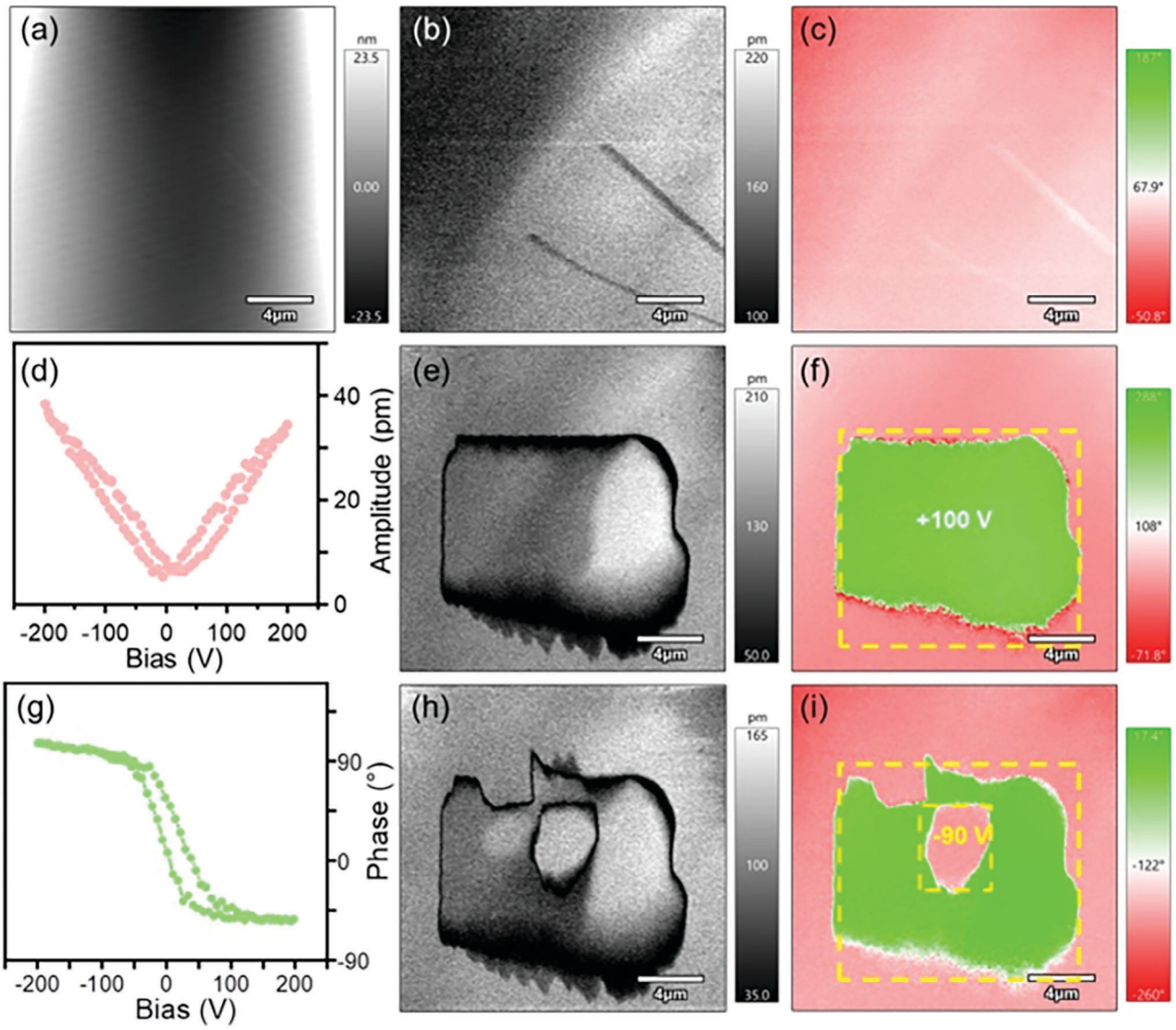

Figure 3. Ferroelectric domain switching behavior of 4-CBZACL. a) PFM topography. b,c) amplitude and phase images for the initial state. d) Hysteretic dependence of the PFM amplitude with applied DC bias detected on the thin single crystal. e,f) after the first electric poling with tip-bias of +100 V on the region of the yellow dashed box. g) Hysteretic dependence of the PFM phase with applied DC bias detected on the thin single crystal. h,i) after the second electric poling with tip-bias of −90 V on the region of the smaller yellow dashed box.

on the *c* axis can be reversed by the rotation of molecules and the distortion of inorganic ions as expected. Furthermore, chloric substitution enlarges the non-coincidence of positive and negative charge, enhancing the polarization. In short, halogen substitution on organic component greatly improves ferroelectric polarization.

3. Conclusion

In summary, we presented a good strategy of molecular engineering that introduces halogen substitution on organic components to enhance the ferroelectric ordering. The experimental results and DFT calculation both reveal that the halogen substitution induce the dipole moment of the organic cations leaning along the direction of spontaneous polarization which results in a huge increase of the P_s (from 13 to 23.3 μC cm^{-2}). In addition, this lead-based ferroelectric semiconductor shows the X-ray detection response with a light/dark current switch. This work presents an easily implemented strategy to improve the ferroelectric performance taking full advantage of the structural adjustability and flexibility of hybrid molecular systems. Meanwhile, it provides an efficient avenue and a good platform for ferroelectricity optimization in the ferroelectric family. Our in-depth insight on the structure-performance relationship also gives more possibility for the role of molecular engineering in other fields.

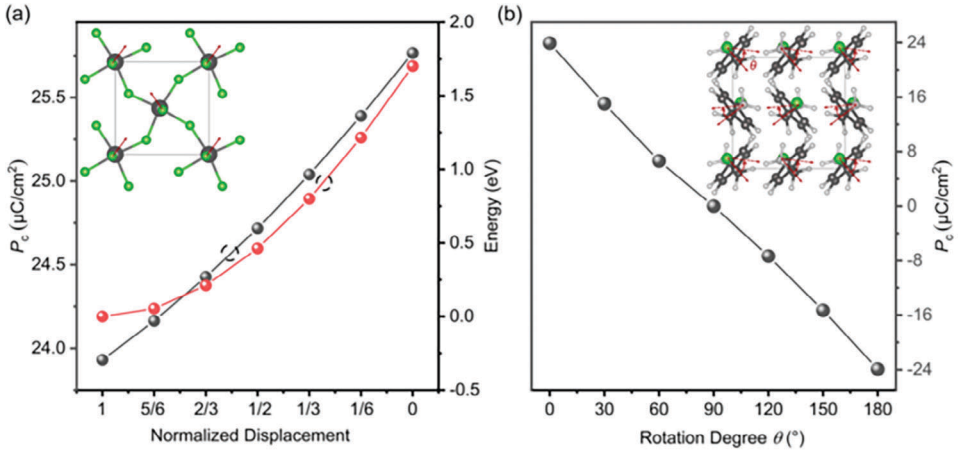

Figure 4. The magnitude polarization along the –*c* axis and energy barrier in two different situations. a) The inorganic ions transform from the ferroelectric state (the normalized displacement is defined as "1") to the paraelectric state (the normalized displacement is defined as "0") gradually and the organic molecular remains in the ferroelectric state. Insert depicts the one-layer inorganic ions $[PbCl_4]^{2-}$ from the top view and the red arrows show the directions of distortion. b) The organic molecular is rotated in the *bc*-plane gradually, and the inorganic ions distort simultaneously. Insert depicts the halogen-substituted organic cations from the top view, and solid red arrows indicate the dipole of organic molecular, and the dashed red arrows indicate the dipole of the rotated molecular characterized by the rotation degree θ.

Supporting Information

Supporting Information is available from the Wiley Online Library or from the author.

Acknowledgements

N.W. and N.D. contributed equally to this work. L.-P.M. acknowledges support from the National Natural Science Foundation of China (Grant No. 22205087) and Open Project Program of Jiangxi Provincial Key Laboratory of Functional Molecular Materials Chemistry, Jiangxi University of Science and Technology, (Grant No. 20212BCD42018). C.S. acknowledges support from the National Natural Science Foundation of China (Grant No. 22175079). H.-Y.Y. acknowledges support from the National Natural Science Foundation of China (Grant No. 21875093) and Natural Science Foundation of Jiangxi Province (Grant Nos. 20204BCJ22015 and 20202ACBL203001). S. D. acknowledges support from the National Natural Science Foundation of China (Grant No. 12274069) and the Big Data Center of Southeast University for providing the computational resource.

Conflict of Interest

The authors declare no conflict of interest.

Data Availability Statement

The data that support the findings of this study are available in the supplementary material of this article.

Keywords

2D, ferroelectric semiconductors, large spontaneous polarization, molecular engineering, organic–inorganic hybrid perovskites

Received: July 31, 2023
Revised: September 21, 2023
Published online: November 2, 2023

[1] Y. Lee, J. Park, S. Cho, Y. E. Shin, H. Ko, *ACS Nano* **2018**, *12*, 4045.
[2] Y. Hu, L. You, B. Xu, T. Li, S. A. Morris, Y. Li, Y. Zhang, X. Wang, P. S. Lee, H.-J. Fan, J. Wang, *Nat. Mater.* **2021**, *20*, 612.
[3] Z. Wen, D. Wu, *Adv. Mater.* **2020**, *32*, 1904123.
[4] S. Han, M. Li, Y. Liu, W. Guo, M.-C. Hong, Z. Sun, J. Luo, *Nat. Commun.* **2021**, *12*, 284.
[5] Z. Hu, M. Tian, B. Nysten, A. M. Jonas, *Nat. Mater.* **2009**, *8*, 62.
[6] Y. Jiang, E. Parsonnet, A. Qualls, W. Zhao, S. Susarla, D. Pesquera, A. Dasgupta, M. Acharya, H. Zhang, T. Gosavi, C.-C. Lin, D. E. Nikonov, H. Li, I. A. Young, R. Ramesh, L. W. Martin, *Nat. Mater.* **2022**, *21*, 779.
[7] S. Wang, T. Zhu, R. Sabatini, A. M. Najarian, M. Imran, R. Zhao, P. Xia, L. Zeng, S. Hoogland, D. S. Seferos, E. H. Sargent, *Adv. Mater.* **2022**, *34*, 2207261.
[8] S. D. Kim, G. T. Hwang, K. Song, C. K. Jeong, K. I. Park, J. Jang, K.-H. Kim, J. Ryu, S. Y. Choi, *Nano Energy* **2019**, *58*, 78.
[9] W. Zhang, R.-G. Xiong, *Chem. Rev.* **2012**, *112*, 1163.
[10] P.-P. Shi, Y.-Y. Tang, P.-F. Li, W.-Q. Liao, Z.-X. Wang, Q. Ye, R.-G. Xiong, *Chem. Soc. Rev.* **2016**, *45*, 3811.
[11] T. Zhang, K. Xu, J. Li, L. He, D.-W. Fu, Q. Ye, R.-G. Xiong, *Natl Sci Rev* **2023**, *10*, nwac240.
[12] Y.-M. You, W.-Q. Liao, D.-W. Zhao, H.-Y. Ye, Y. Zhang, Q.-H. Zhou, X.-H. Niu, J.-L. Wang, P.-F. Li, D.-W. Fu, Z.-M. Wang, S. Gao, K.-L. Yang, J.-M. Liu, J.-Y. Li, Y.-F. Yan, R.-G. Xiong, *Science* **2017**, *357*, 306.
[13] L. Qi, S.-C. Ruan, Y.-J. Zeng, *Adv. Mater.* **2021**, *33*, 2005098.
[14] W.-L. Zheng, X.-C. Wang, X. Zhang, B. Chen, H. Suo, Z.-F. Xing, Y.-Z. Wang, L.-H. Wei, J.-K. Chen, Y. Guo, F. Wang, *Adv. Mater.* **2023**, *35*, 2205410.
[15] R. Ding, Y. X. Lyu, Z.-H. Wu, F. Guo, W. F. Io, S.-Y. Pang, Y.-Q. Zhao, J.-F. Mao, M.-C. Wong, J.-H. Hao, *Adv. Mater.* **2021**, *33*, 2101263.
[16] H.-J. Xu, S.-G. Han, Z.-H. Sun, J.-H. Luo, *Acta Chim. Sin. (Engl. Ed.)* **2021**, *79*, 23.
[17] P. Siwach, P. Sikarwar, J. S. Halpati, A. K. Chandiran, *J. Mater. Chem. A* **2022**, *10*, 8719.
[18] N. Mercier, N. Louvain, W.-H. Bi, *CrystEngComm* **2009**, *11*, 720.
[19] C.-F. Wang, H. Li, M.-G. Li, Y. Cui, X. Song, Q.-W. Wang, J.-Y. Jiang, M.-M. Hua, Q. Xu, K. Zhao, H.-Y. Ye, Y. Zhang, *Adv. Funct. Mater.* **2021**, *31*, 2009457.

[20] L.-N. Li, X.-T. Liu, Y.-B. Li, Z.-Y. Xu, Z.-Y. Wu, S.-G. Han, K.-W. Tao, M.-C. Hong, J.-H. Luo, Z.-H. Sun, *J. Am. Chem. Soc.* **2019**, *141*, 2623.
[21] Y. Chen, C. Gao, T. Yang, W. Li, H. Xu, Z. Sun, *Chin. J. Struct. Chem.* **2022**, *41*, 2204001.
[22] Y. Sun, G. Niu, W. Ren, X. Meng, J. Zhao, W. Luo, Z.-G. Ye, Y.-H. Xie, *ACS Nano* **2021**, *15*, 10982.
[23] H. Wei, Y. Yang, S. Chen, H. J. Xiang, *Nat. Commun.* **2021**, *12*, 637.
[24] N. Leblanc, N. Mercier, L. Zorina, S. Simonov, P. Auban-Senzier, C. Pasquier, *J. Am. Chem. Soc.* **2011**, *133*, 14924.
[25] W.-Q. Liao, Y. Zhang, C.-L. Hu, J.-G. Mao, H.-Y. Ye, P.-F. Li, S.-D. Huang, R.-G. Xiong, *Nat. Commun.* **2015**, *6*, 7338.
[26] L. Li, X. Liu, C. He, S. Wang, C. Ji, X. Zhang, Z. Sun, J. Luo, *J. Am. Chem. Soc.* **2020**, *142*, 1159.
[27] C.-R. Huang, X. Luo, X.-G. Chen, X.-J. Song, Z.-X. Zhang, R.-G. Xiong, *Natl Sci Rev* **2021**, *8*, nwaa232.
[28] H.-Y. Zhang, Y.-Y. Tang, P.-P. Shi, R.-G. Xiong, *Acc. Chem. Res.* **2019**, *52*, 1928.
[29] H.-Y. Zhang, Z.-X. Zhang, X.-J. Song, X.-G. Chen, R.-G. Xiong, *J. Am. Chem. Soc.* **2020**, *142*, 20208.
[30] M. A. Spackman, D. Jayatilaka, *CrystEngComm* **2009**, *11*, 19.
[31] M. A. Spackman, J. J. McKinnon, *CrystEngComm* **2002**, *4*, 378.
[32] Y.-P. Fu, S. Jin, X.-Y. Zhu, *Nat. Rev. Chem.* **2021**, *5*, 838.
[33] M. E. Lines, A. M. Glass, *Principles and Applications of Ferroelectrics and Related Materials*, Oxford university press, Oxford, UK **2001**.
[34] K. Aizu, *J. Phys. Soc. Jpn.* **1969**, *27*, 387.
[35] J. Wang, Y. Ma, Z. Wang, X. Liu, S. Han, Y. Liu, W. Guo, J. Luo, Z. Sun, *Matter* **2022**, *5*, 194.
[36] C. Ji, S. Wang, Y. Wang, H. Chen, L. Li, Z. Sun, Y. Sui, S. Wang, J. Luo, *Adv. Funct. Mater.* **2020**, *30*, 1905529.
[37] Y.-K. Li, T.-T. Ying, H. Zhang, Y.-H. Tan, Y.-Z. Tang, F.-X. Wang, M.-Y. Wan, *Dalton Trans.* **2022**, *51*, 6860.
[38] X.-G. Chen, X.-J. Song, Z.-X. Zhang, H.-Y. Zhang, Q. Pan, J. Yao, Y.-M. You, R.-G. Xiong, *J. Am. Chem. Soc.* **2020**, *142*, 10212.
[39] I. H. Park, Q. Zhang, K. C. Kwon, Z. Zhu, W. Yu, K. Leng, D. Giovanni, H. S. Choi, I. Abdelwahab, Q.-H. Xu, T. C. Sum, K. P. Loh, *J. Am. Chem. Soc.* **2019**, *141*, 15972.
[40] X.-G. Chen, X.-J. Song, Z.-X. Zhang, P.-F. Li, J.-Z. Ge, Y.-Y. Tang, J.-X. Gao, W.-Y. Zhang, D.-W. Fu, Y.-M. You, R.-G. Xiong, *J. Am. Chem. Soc.* **2020**, *142*, 1077.
[41] H.-Y. Zhang, X.-J. Song, X.-G. Chen, Z.-X. Zhang, Y.-M. You, Y.-Y. Tang, R.-G. Xiong, *J. Am. Chem. Soc.* **2020**, *142*, 4925.
[42] M. Mączka, J. K. Zareba, A. Gagor, D. Stefańska, M. Ptak, K. Roleder, D. Kajewski, A. Sieradzki, *Chem. Mater.* **2021**, *33*, 2331.
[43] C. K. Yang, W. N. Chen, Y. T. Ding, J. Wang, Y. Rao, W. Q. Liao, Y.-Y. Tang, P.-F. Li, Z.-X. Wang, R. G. Xiong, *Adv. Mater.* **2019**, *31*, 1808088.
[44] K. Ding, H. Ye, C. Su, Y.-A. Xiong, G. Du, Y.-M. You, Z.-X. Zhang, S. Dong, Y. Zhang, D.-W. Fu, *Nat. Commun.* **2023**, *14*, 2863.